Green Chemistry

PAPER

View Article Online
View Journal | View Issue

Cite this: *Green Chem.*, 2015, **17**, 4800

Interfacial improvements in biocomposites based on poly(3-hydroxybutyrate) and poly(3-hydroxybutyrate-*co*-3-hydroxyvalerate) bioplastics reinforced and grafted with α-cellulose fibers†

Liqing Wei,[a] Nicole M. Stark[b] and Armando G. McDonald*[a]

In this study, α-cellulose fibers reinforced green biocomposites based on polyhydroxybutyrate (PHB) and the copolymer poly(3-hydroxybutyrate-*co*-3-hydroxyvalerate) (PHBV) were prepared and characterized. The α-cellulose fibers were isolated from at-risk intermountain lodgepole pine wood by successive removal of extractives, lignin and hemicellulose. Grafting of PHB or PHBV onto cellulose was conducted using reactive extrusion with dicumyl peroxide free radical initiation at high temperature. It is postulated that the grafted copolymers at the interfaces of cellulose and the polymer matrix performed as an interfacial coupling agent. Grafting tended to interact with both the hydrophilic fibers and the hydrophobic PHB or PHBV matrix. The biocomposites were characterized by scanning electron microscopy (SEM) and dynamic mechanical analysis (DMA) and indicated good interfacial bonding and compatibility between the two phases. The mechanical properties of the biocomposites were improved by grafting due to improved stress transfer between the two interphases of the fiber/polymer matrix as compared to the blend control composite. The crystallinity of PHB, PHBV and cellulose in the biocomposite were reduced as determined by Fourier transform infrared spectroscopy (FTIR), wide-angle X-ray diffraction (WAXD), and differential scanning calorimetry (DSC) analyses. This *in situ* reactive extrusion process offers an effective approach to improve the properties of biocomposite materials from sustainable resources.

Received 10th July 2015,
Accepted 3rd August 2015

DOI: 10.1039/c5gc01568e

www.rsc.org/greenchem

1. Introduction

Strong, lightweight, and moldable plastics are used in thousands of products that improve the quality of life and bring convenience to our everyday lives. However, at least 40% of these conventional (petroleum-based) plastics are used in short-term applications (*e.g.* throwaway cups, utensils, plastic bags) and after being disposed the resulting waste can quickly lead to both terrestrial and marine environmental pollution.[1,2] In brief, petroleum-based plastics are not sustainable, which drives the efforts to develop more environmentally benign plastics and materials. Some of the most commonly known bio-based and biodegradable plastics from renewable resources include polylactic acid (PLA), polyhydroxyalkanoates [PHAs, *e.g.* polyhydroxybutyrate (PHB) and poly(hydroxybutyrate-*co*-hydroxyvalerate) (PHBV)], thermoplastic starch, protein based plastics and the most abundant terrestrial polymer on earth, cellulose and its derivatives.[3,4] Extensive application of these bioplastics, notably PHB and PHBV, will occur only after overcoming challenges including poor melt elasticity, low thermal degradation temperature, high crystallinity leading to brittleness for PHB, and low crystallization rate of PHBV.[5,6] These features, especially low melt elasticity, limit their processability window, for example, during extrusion processes typically used for film, injection molding, blown-film manufacture, thermoforming, and fiber spinning.[5,7]

Another critical issue is the millions of acres of forestland that have become prone to disease and insect attack in the Inland-Northwest of the United States, and high risk for catastrophic wildfire because of overstocked stands.[8] Approximately 6 million dry tons of sound dead wood from Idaho's National Forests is available. Of this, a sustainable level of over one million dry tons per year of logging residues and thinnings are potentially available for producing a variety of bio-

[a]*Renewable Materials Program, Department of Forest, Rangeland and Fire Sciences, University of Idaho, Moscow, Idaho 83844-1132, USA*
[b]*U.S. Department of Agriculture, Forest Service, Forest Products Laboratory, One Gifford Pinchot Drive, Madison, Wisconsin 53726-2398, USA.*
E-mail: armandm@uidaho.edu; Fax: +1 (208) 885 6564; Tel: +1 (208) 885 9454
†Electronic supplementary information (ESI) available. See DOI: 10.1039/c5gc01568e

products. Therefore, there is a need to generate materials, such as cellulose, from this abundant woody biomass for use in value-added products.

Wood fibers have been used as fillers in thermoplastics to produce wood plastic composites (WPCs), which can be used in various applications (decks, railings and automotive) due to their well acceptable properties, low costs, and renewability.[9] WPC performances can be further improved by exchanging wood fiber for cellulose fiber based on its improved thermal stability and mechanical properties. Cellulose fibers have been widely used as reinforcing fillers in conventional thermoplastics, such as polypropylene and polyethylene.[10–13] Some mechanical properties, such as Young's modulus and tensile strength, were improved due to the addition of cellulose fibers.[12] However, the presence of a large number of hydroxyl groups results in a polar fiber surface; it is very difficult to disperse polar cellulose in a non-polar polymer matrix. This difficulty can result in poor interfacial bonding between the cellulose and the polymer matrix. Poor adhesion at the interface means that the full capabilities of the composite cannot be exploited and leads to low mechanical properties and a reduced life span.[11] Due to this reason, cellulose performs as a simple filler and not as a true reinforcing agent. Research to improve the interfacial adhesion of biocomposites continues. Extensive studies have been conducted using coupling agents (*e.g.* maleated-polypropylene and maleated-polyethylene) to enhance the interfacial adhesion of the fiber filler and the polymer matrix.[14] Other efforts including chemical/physical treatments of fiber fillers to reduce the hydrophilicity of cellulose fiber surfaces have gained much more attention.[15–18] Although these modifications result in a decrease in moisture absorption and an increase in mechanical properties, biodurability and weatherability, the processes used for cellulose modification are costly and involve toxic chemicals which could be a deterrent to its use.[9,19]

By exchanging conventional plastics (*e.g.* polyethylene and polypropylene) with bioplastics (*e.g.* PHB and PHBV), which are less hydrophobic, will produce a fully bio-based composite material that is sustainably derived with good mechanical properties (flexural/tensile strength and stiffness) and biodegradation behaviors.[17,20–22] Additionally, biocomposite properties can be improved by incorporating modified cellulose fibers into a bioplastic matrix.[23–25] Recently, the reaction mechanism of a "grafting onto" method has been successfully studied by grafting the PHB polymer onto cellulose fibers through the reactive extrusion processing with the use of a small amount of peroxide (Fig. 1).[26] When the peroxide is exposed to heat during extrusion it will decompose into strong free radicals which tend to abstract H's from the polymer and cellulose molecular chains and initiate the grafting between the two phases in composites. *Via* the strategy of grafting PHB or PHBV onto cellulose this will retain the stiffness of cellulose and the flexibility of the polymer matrix (PHBV especially). In addition, the use of reactive extrusion which limits the use of

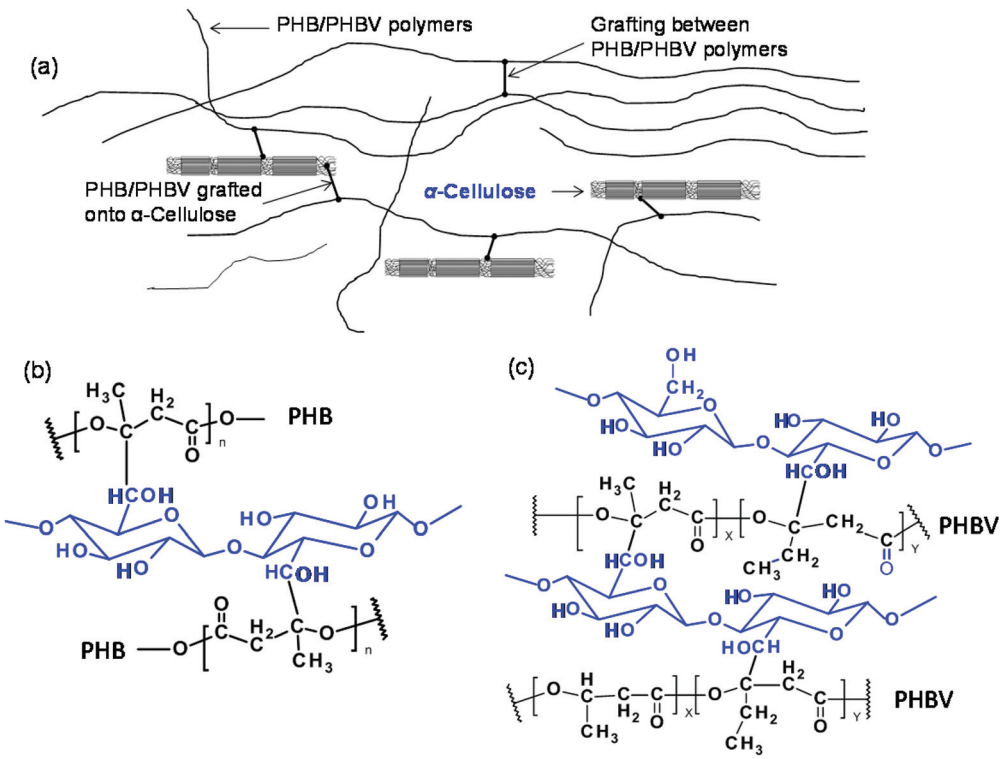

Fig. 1 Generalized schematic representation of grafted PHB or PHBV polymers onto αCell (a), and the chemical structures of grafted αCell-*g*-PHB (b) and αCell-*g*-PHBV (c) biocomposites.

solvents and the treatment of cellulose, makes it a valuable alternative to improve the performances of cellulose reinforced bioplastic composites. Chemically coupling PHB to cellulose fiber provides excellent stress transfer and hydrophobic–hydrophilic compatibility between the two phases in the biocomposite material with no external non-biodegradable coupling agents or compatibilizers are employed. This in-line modification process can be applied easily to industrial scale production of biocomposites.

Our aim in this study was to isolate α-cellulose (αCell) fibers from at-risk lodgepole pine wood. The "grafting onto" strategy was used to prepare cellulose-*graft*-PHBV (αCell-*g*-PHBV) or αCell-*g*-PHB biocomposites with improved properties due to enhanced interfacial adhesion. The surface morphology, chemistry, and crystalline structure of the modified biocomposites were characterized by microscopy, Fourier transform infrared (FTIR) spectroscopy, and wide angle X-ray diffraction (WAXD), respectively. Tensile tests were conducted on the injection molded dog-bone specimens. Thermal properties, such as thermal transition and crystallinity, thermal degradation, dynamic flexural properties, and thermal mechanical properties of biocomposites were assessed by thermal analysis.

2. Results and discussion

2.1. α-Cellulose fiber analysis

The chemical composition of the original wood and αCell fibers for CH_2Cl_2 extractive, lignin, and carbohydrate content/composition was determined and shown in Table 1.[27] Lodgepole pine wood was composed of 39% cellulose. After isolation, αCell had a 96% purity based on the glucose content.

The αCell fiber size (weight) distribution was determined using an automatic vibratory sieve shaker. As shown in Table 2, the major part of the αCell fiber was smaller than 250 μm, with 65% of the fibers between 70 and 177 μm. Further information concerning αCell fiber size (length and diameter) was achieved by optical microscopy. The micrographs of each screened fraction are shown in Fig. 2. Single fibers were observed (rod like), especially for the fractions that were >60 mesh (Fig. 2c–f). The length (L) and diameter (d) of these fiber fractions were measured and averaged from 200 fibers. The weight normalized fiber L and d were 0.5 mm and 15.1 μm, respectively. The L of the >80, >100, and >200 mesh classified fibers ranged between 0.6 and 0.8 mm, while the d of these fractions were comparable around 19 μm. The fine fractions (<200 mesh) had a much smaller L (0.4 mm) and d (14 μm) than the coarser fractions. The 40 and 60 mesh fractions comprised fiber bundles (Fig. 2a and b); hence the fiber length and diameter were difficult to be determined. As shown in Table 2, 59% (weight fraction) of the αCell fibers had an aspect ratio (L/d) of 31 and is considered microcrystalline.[28] The aspect ratio was shown to decrease with a finer mesh size.

Table 1 Chemical composition of the lodgepole pine wood and isolated αCell fibers (dry basis)

Composition	Lodgepole pine wood (%)	α-Cellulose (%)
Cellulose	39.1	95.9
Glucan 6C	39.1	95.9
Hemicellulose	33.1	3.9
Xylan 5C	5.3	3.8
Galactan 6C	11.5	0.0
Mannan 6C	16.3	0.1
Arabinan 5C	1.5	0.0
Lignin	26.9	0.2
Klason lignin	26.5	0.2
Acid soluble lignin (ASL)	0.4	0.0
CH_2Cl_2 extractives	1.7	0.0
Ash	0.01	0.0

2.2. Reaction conditions optimization and grafting efficiency

The effect of two factors (DCP concentration: 2–5%; reaction time, t_R: 5–15 min) was investigated to optimize the grafting efficiency between the αCell and the PHB (or PHBV) polymer matrix. The extruded composite strands were extracted with $CHCl_3$ to remove any nonreacted PHB/PHBV or smaller homopolymer molecules and then filtered to remove the nongrafted αCell fibers (Note: CH_2Cl_2 and $CHCl_3$ used in this research were recovered for reuse to reduce environmental impact). The dry weight of the copolymer gels was recorded and gel% was calculated with respect to the dry weight of the starting materials. The optimized total concentration of DCP and t_R were 2% and 10 min, respectively, to give the maximum αCell-*g*-PHB and αCell-*g*-PHBV copolymer gel% and well mixed biocomposites samples. The degree of grafting efficiency (GE%, weight% of PHBV (or PHB)) grafted onto the αCell backbone was calculated),

$$\mathrm{GE}\% = (W_{\mathrm{gf}} - W_{\alpha\mathrm{Cell}})/W_{\mathrm{PHB/PHBV}} \times 100 \quad (1)$$

where W_{gf}, $W_{\alpha Cell}$, and $W_{PHB/PHBV}$ are the weights of the grafted copolymer gel recovered after Soxhlet extraction, initial αCell, and initial PHB (or PHBV) weights, respectively.[19] The simple blended composites were also extracted in the same way as grafted samples. The GE% of simple blends was <0.5%, and thus being neglected in this study. The highest GE% value of αCell with PHBV was 45% but that with PHB was 35%, when biocomposites were processed under the same optimized reactive conditions (DCP: 2 wt%; t_R: 10 min). As shown in Fig. 1, the grafting reactions occurred at the tertiary –CH sites of PHB and PHBV. The PHBV copolymer has one additional tertiary –CH site in each comonomeric unit as compared with the PHB, therefore, higher GE% was observed for αCell-*g*-PHBV copolymers. It is worth noting that the high GE% can also be ascribed to partial crosslinking/grafting of the polymer matrices (Fig. 1a).

2.3. Surface morphology of biocomposites

The SEM micrographs of the biocomposite surfaces are shown in Fig. 3. The grafted biocomposites (Fig. 3b and d) showed a

Table 2 Yield of each fraction of αCell fibers retained on sieves with various openings, and the averaged fiber length, diameter, and the aspect ratio measured by microscopic analysis

Retained on mesh	Sieve opening (μm)	Particle weight fraction (%)	Fiber length (L, mm)[a]	Fiber diameter (d, μm)[a]	Aspect ratio (L/d)
40	420	7.3	—	—	—
60	250	6.3	—	—	—
80	177	16.0	0.8 ± 0.1	19.0 ± 1.6	42.1
100	149	11.4	0.7 ± 0.1	18.7 ± 2.8	37.4
200	70	37.5	0.6 ± 0.1	18.5 ± 2.0	32.4
<200	<70	21.5	0.4 ± 0.1	14.0 ± 2.1	28.6
Average			0.5	15.1	29.3

[a] The fiber length and diameter of αCell fibers of the 60 and 40 mesh fractions could not be accurately determined due to fiber bundles as shown in Fig. 2a and b.

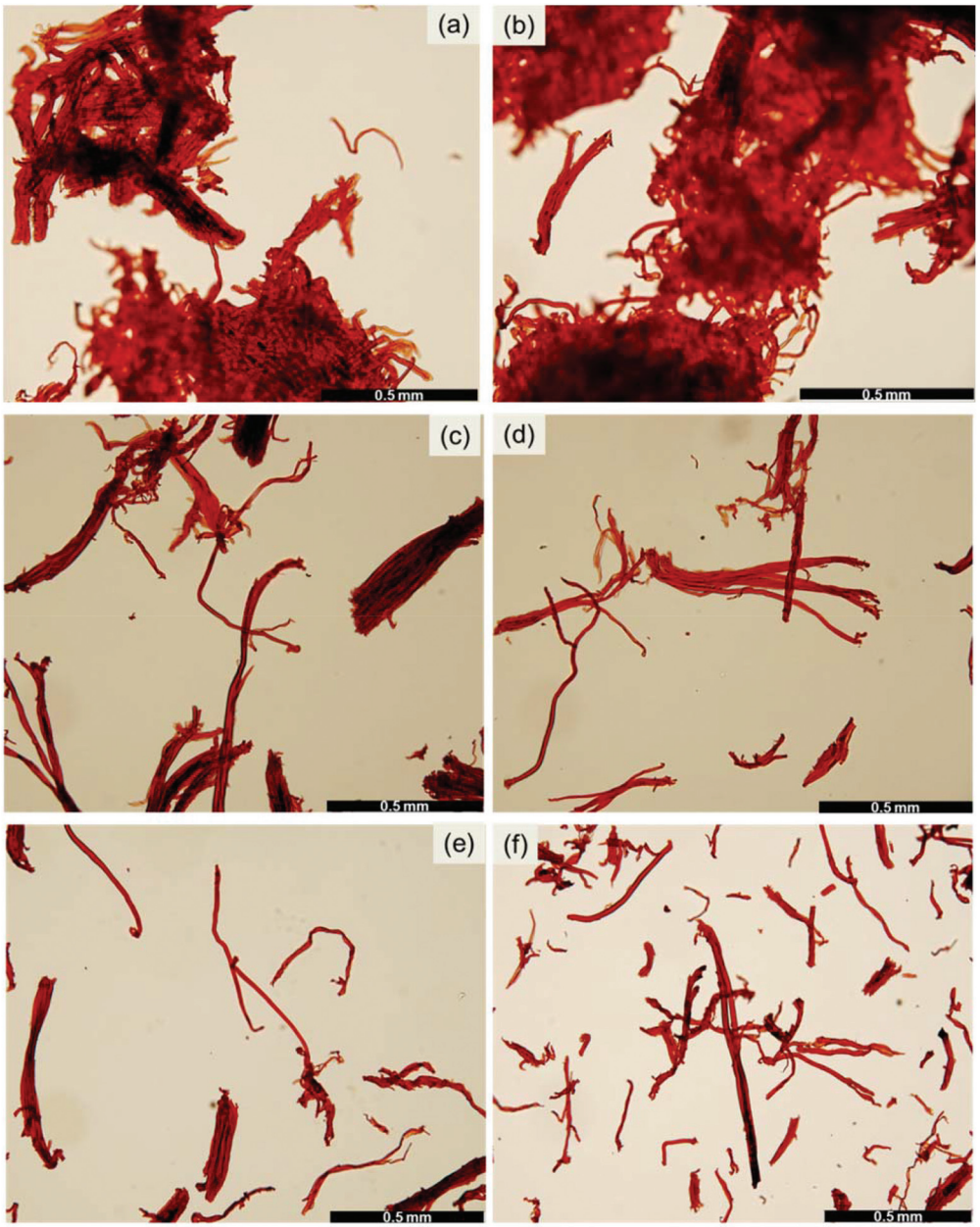

Fig. 2 Optical micrographs of αCell fibers fractions classified (a) >40 mesh, (b) >60 mesh, (c) >80 mesh, (d) > 100 mesh, (e) > 200 mesh and (d) <200 mesh.

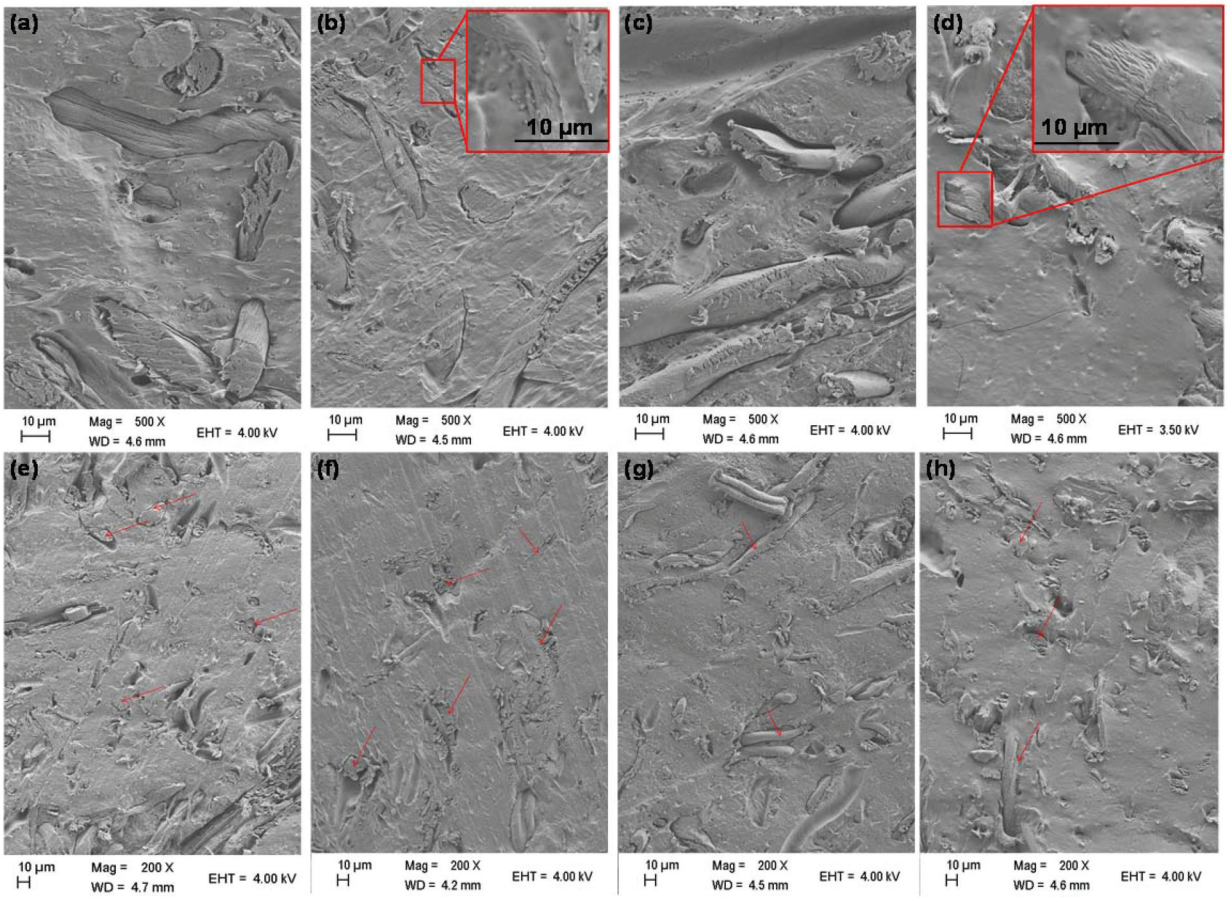

Fig. 3 SEM micrographs of surface morphologies of αCell-PHB (a: 500×; e: 200×), αCell-*g*-PHB (b: 500×; f: 200×), αCell-PHBV (c: 500×; g: 200×), and αCell-*g*-PHBV (d: 500×; h: 200×) composites. Note: fiber and the polymer matrix interface was shown in in-set micrographs with larger magnification (1000×) of the grafted composites (b and d); fibers are pointed out by arrows.

continuous interphase between fiber and the polymer matrix, indicating that the polymer was grafted onto αCell by peroxide initiation. In contrast, blends of αCell-PHB and αCell-PHBV showed discrete zones of PHB or PHBV and αCell fibers (Fig. 3a and c), and the fibers were easily pulled out from the matrix when microtomed. A similar trend was observed with peroxide treated sisal fibers filled in the polyethylene composites system.[29] An improved compatibility between αCell and the polymer matrix was obtained due to peroxide induced grafting (Fig. 3b and d). It was therefore postulated that the grafted copolymer formed on the interfaces of αCell and PHBV (or PHB) coupled the hydrophilic αCell to the hydrophobic PHBV (or PHB) matrix (Fig. 1). Micrographs at a magnification of 200× (Fig. 3e–h) showed the cellulose fibers that have been separated during the mixing extrusion process are well dispersed in the polymer matrices, especially in the grafted composites as compared to the simple blends. On average a random orientation of cellulose fibers into the polymer matrices for both grafting as well as their simple blends was observed. However, the surfaces of αCell fibers became rougher and more amorphous due to peroxide treatment, which may provide higher possibility of access for melted polymers to attach onto during composites processing. This further suggested better interfacial adhesion between αCell fibers and PHB (or PHBV) was due to grafting.

2.4. Characterization of biocomposites by FTIR and XRD

The crystalline nature of PHB and its composite materials significantly affect their mechanical properties and processability as well. Copolymerization of 3-hydroxybutyrate with other monomeric units, such as 3-hydroxyvalerate (3HV), to form PHBV copolymers has been proven to be one of the most effective strategies to reduce the crystallinity of PHB. These copolymers showed improved mechanical properties as a result of being less crystalline, which contributed to the presence of dislocations, crystal strain and smaller crystallite sizes due to the disruption of 3HV unit to PHB crystal lattice.[30] The degree of crystallinity of PHB and PHBV can be obtained by a combination of FTIR and WAXD analyses. Fig. 4a showed the FTIR spectra of the composite samples with characteristic absorbance peaks arising from αCell and PHBV (or PHB). The absorbance bands at 980, 1230, and 1720 cm^{-1} were assigned to the crystalline regions of PHB or PHBV polymers, and as expected the intensities of these peaks were lower for PHBV

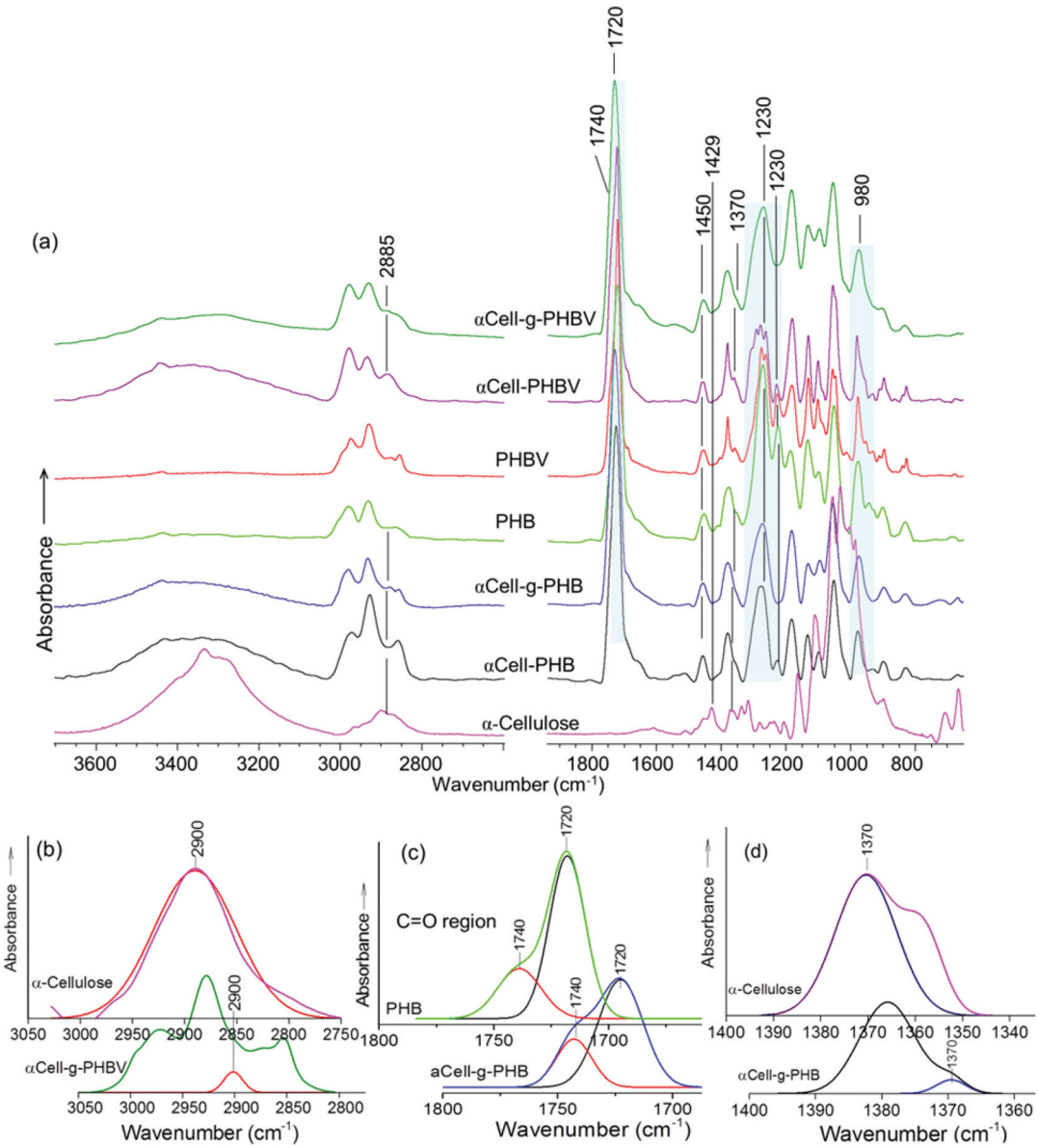

Fig. 4 (a) FTIR spectra for α-cellulose, PHB, PHBV, and their composites samples; (b) –C–H stretching (2900 cm^{-1}) fitted bands for αCell and αCell-*g*-PHBV composites; (c) carbonyl (C═O) fitted peaks for PHB and αCell-*g*-PHB composites, and (d) –C–H bending (1370 cm^{-1}) fitted peaks for αCell and αCell-*g*-PHB composites.

based samples than those of PHB's. This further indicated that the copolymer PHBV was less crystalline than PHB. It was shown that the intensities of these crystalline bands for the grafted composites were reduced significantly, due to grafting, compared to their simple blends (αCell-PHB and αCell-PHBV). The shoulder at 1740 cm^{-1} of the band centered at 1720 cm^{-1} was assigned to the carbonyl (C═O stretching) group from the amorphous region of PHB and PHBV, and it became more intense after grafting (see the peak fitting of the C═O region shown in Fig. 4c). This observation suggested that successful grafting between the matrix (PHB and PHBV) and αCell reinforcement was achieved, which would hinder the crystallization of PHBV (or PHB) macromolecular chains from melts, resulting in a higher proportion of amorphous PHBV (or PHB). It is worth noting that the reduction of crystallinity of grafted composites could also be attributed to the crosslinking of the polymer matrix (PHB–PHB or PHBV–PHBV). In addition, due to the high degree of crystallinity/rigidity with the less mobile cellulose, only radicals formed on the surfaces of its crystalline and amorphous regions would be more accessible to the molten PHB/PHBV (with radicals) which would then be able to form grafts in the composites. Therefore, the band at 1429 cm^{-1} (symmetric $–CH_2$ bending), a characteristic of amorphous cellulose, which appeared in the grafted composites, again providing further evidence that grafting had occurred. To further confirm that the crystallinity was reduced due to

grafting, quantitative analyses of the spectra for PHBV (and PHB) and cellulose crystallinity were performed. The spectral ratio of 1370/2900 cm^{-1} bands (total crystallinity index, TCI, eqn (3)) was shown to be proportional to the crystallinity degree of cellulose, while the band ratios 1720/1740 cm^{-1} (carbonyl index, $I_{C=O,PHB/PHBV}$, eqn (4)) and 1230/1450 cm^{-1} (C–O index, $I_{C-O,\ PHB/PHBV}$, eqn (5)) reflect the crystallinity of PHB or PHBV polymers. Quantitative analyses of the infrared crystallinity ratios were calculated from the peak fitted spectra of the –C–H (and $-CH_2$ stretching) at 2900 cm^{-1} (Fig. 4b), the carbonyl region (1800–1680 cm^{-1}) for PHB (Fig. 4c), and –C–H bending centered at 1370 cm^{-1} from the crystalline region for cellulose (Fig. 4d). The analyzed data for neat PHB and PHBV, αCell, αCell-PHB blend, αCell-PHBV blend, and grafted composites (αCell-*g*-PHB and αCell-*g*-PHBV) are given in Table 4. The addition of αCell resulted in a reduction in PHBV (and PHB) crystallinity of the blended composites slightly, while grafting reduced all the three crystallinity indices significantly. The grafted copolymers between the αCell and PHBV (or PHB) matrix had improved compatibility, which would improve the stress transfer between the two phases of hydrophilic cellulose and the hydrophobic polymer.[26]

To further investigate the effect of the grafting on the crystalline structures of PHB and cellulose segments, vacuum dried samples were subjected to WAXD analysis (Fig. 5). αCell showed four crystalline peaks corresponding to (101), (10−1), (002), and (040) planes shown at the 2θ scale of 14°, 16°, 22°, and 35°, respectively. The maximum diffractogram intensity was observed in the (002) plane. This is a typical pattern of cellulose I. Both PHB and PHBV samples showed crystalline peaks at 2θ near to 13°, 17°, 20°, 21°, 22°, 26° and 27°, respectively, ascribing to planes of (020), (110), (021), (101), (121), (040), and (200). The most intense peak for PHB and the composite samples was at 17°, whereas the most intense peak for PHBV based samples was observed at 13°. It is assumed that the reduced crystallinity of PHBV as compared to PHB could be the main contributor to peak broadening for all the crystalline planes. Such results can be explained by the fact that the presence of αCell suppressed the nucleation of the polymer, especially for PHBV, in the simple blends. The similar reduction of PHB and PHBV crystallinity was also found in PHB/cellulose (Whatman CF1) and PHBV/PLA/PBS (poly(butylene succinate)) blends, respectively.[26]

The Gaussian function was used for peak fitting of the WAXD diffractograms, meantime, the FWHM values were obtained accordingly. Crystallinity indices were calculated from the ratios of fitted peak intensities, and crystal sizes according to Scherrer's formula using a shape constant $K = 0.9$ for PHBV (and PHB) and cellulose (Table 3). The crystallinity index[19] and average crystal width were 59.1% ($CrI\%_{\alpha Cell}$, eqn (6)) and 250 Å (D_{002}) for αCell, 61% ($CrI\%_{PHB}$, eqn (7)) and 1274 Å (D_{020}) for PHB, and 36.2% ($CrI\%_{PHBV}$, eqn (8)) and 190 Å (D_{020}, eqn (9)) for PHBV, respectively. PHBV had a much smaller crystal size and a significantly lower degree of crystallinity than PHB based materials. The lower crystallinity for PHBV would result in a more ductile/flexible material than PHB. The large crystal size which would induce inter-spherulitic cracks is one of the leading reasons for the brittleness of PHB.[31,32] The simple blending of PHB (or PHBV) with αCell was shown to reduce slightly the crystallinity indices and crystal sizes of the PHB (or PHBV) polymer. Nevertheless, the decreasing trend was more significant as a result of grafting (Table 3), which contributed to new C–C bonds being formed which limited the numbers of PHB or PHBV molecular chains involved in crystallization processes from the polymer melt. The PHB and PHBV molecular chains with more grafted sites would contribute to an increase in the amorphous component due to inhibited crystallization. These results were consistent with the findings from infrared crystallinity indices results and supported the lowering in crystallinity of the polymer matrix by grafting. Smaller crystal sizes of the grafted biocomposites were observed suggesting that the formation of large crystals of either PHBV or PHB was restricted. This could be one of the major reasons for the improved mechanical properties of grafted biocomposites as compared to the simple blends of cellulose and a polymer (PHB or PHBV).

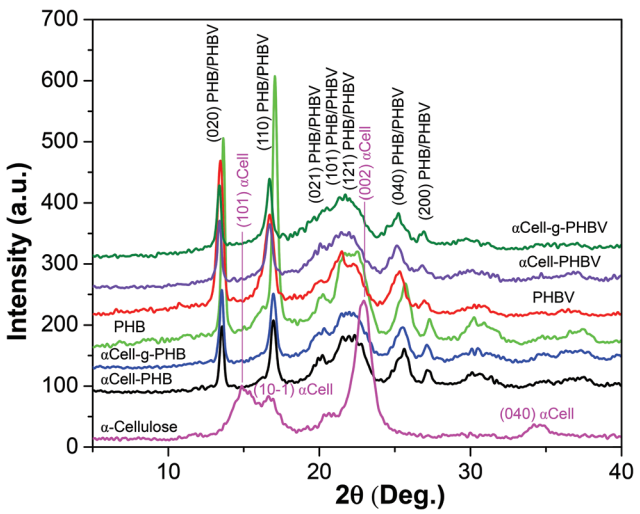

Fig. 5 XRD diffractograms of αCell, PHB, PHBV, blended composite (αCell-PHB and αCell-PHBV) and grafted composite (αCell-*g*-PHB and αCell-*g*-PHBV) samples.

2.5. Influence of grafting on mechanical properties of biocomposites

The density (ρ) and tensile properties (strength (σ), modulus (E), elongation at break (ε), and energy at break (EAB)) of molded neat bioplastics and their composites are given in Table 4. The ρ of all PHB, PHBV and biocomposites samples ranged from 1.10 to 1.18 g cm^{-3} and thus was not a major factor causing differences in tensile properties between treatments. The density of the biocomposites remains similar to neat plastics, which may be because the density of cellulose fiber was about 1.5 g cm^{-3} and only 20% of cellulose was used in the composites.

Table 3 Crystallinity parameters characterized by FTIR and WAXD[a]

	FTIR			WAXD			
Sample	$TCI_{\alpha Cell}$	$I_{C=O,\ PHB/PHBV}$	$I_{C-O,\ PHB/PHBV}$	$CrI\%_{\alpha Cell}$	$CrI\%_{PHB/PHBV}$	D (002) (Å)	D (020) (Å)
αCell	0.4	—	—	59.1	—	250	—
PHB	—	3.8	2.0	—	61.0	—	1274
αCell-PHB	0.3	3.3	0.6	56.4	57.9	233	1108
αCell-*g*-PHB	0.1	2.2	0.4	33.9	45.4	90	312
PHBV	—	2.7	0.8	-	36.2	90	190
αCell-PHBV	0.3	2.6	0.4	40.2	34.2	82	153
αCell-*g*-PHBV	0.1	1.8	0.1	28.7	26.4	40	97

[a] Crystal sizes were determined in the direction perpendicular to the planes of (002) and (020) for αCell and polymers PHB and PHBV, respectively.

Table 4 Density (ρ), tensile strength (σ), tensile (Young's) modulus (E), elongation at break (ε), and energy at break (EAB) of molded neat PHB/PHBV and their biocomposites samples (10 replicates). Standard deviation values are given in parentheses. Samples with the same letter are not significantly different at 95% confidence interval of probability using Tukey's paired t-tests

Sample	ρ (g cm^{-3})	E (GPa)	σ (MPa)	ε (%)	EAB (J)
Neat PHB	1.18 (0.02)^{abc}	2.2 (0.3)^{a}	23.1 (3.3)^{a}	13.6 (1.0)^{a}	0.33 (0.03)^{a}
αCell-PHB	1.14 (0.03)^{abc}	2.6 (0.2)^{ab}	25.9 (1.4)^{ab}	11.2 (0.3)^{b}	0.41 (0.03)^{b}
αCell-*g*-PHB	1.10 (0.02)^{abc}	5.5 (0.7)^{c}	28.1 (1.8)^{c}	13.2 (2.0)^{ac}	0.60 (0.05)^{c}
Neat PHBV	1.18 (0.01)^{def}	0.9 (0.1)^{d}	11.8 (2.0)^{d}	19.6 (1.8)^{d}	0.45 (0.03)^{d}
αCell-PHBV	1.10 (0.02)^{def}	1.3 (0.1)^{e}	13.9 (2.5)^{e}	15.4 (1.8)^{e}	0.53 (0.05)^{e}
αCell-*g*-PHBV	1.06 (0.02)^{def}	2.4 (0.3)^{f}	15.9 (1.7)^{f}	18.8 (1.0)^{df}	0.76 (0.05)^{f}

According to Maldas and Kokta,[33] the mechanical properties of short-fibers and plastic composites are strongly influenced by the fiber content, fiber morphology (size and shape), the orientation (random or unidirectional) of the fillers, and the fiber–polymer adhesion. The σ is more dependent on the fiber–polymer interaction (compatibility) while E is dependent more on the fiber content and morphology (*i.e.* aspect ratio).[14] The grafted biocomposites resulted in an increase of E and σ. The E values of αCell-PHB and αCell-PHBV biocomposites were higher than those of the neat PHB and PHBV, respectively. This indicated the reinforcement effect of cellulose fibers on the polymer matrices. On the other hand, the increments of E were much more significant for the grafted composites due to grafting between cellulose and polymer matrices. The neat PHBV and blended αCell-PHBV composite showed lower E as compared to PHB and blended αCell-PHB, which was attributed to the lower tensile properties of PHBV.[34] Whereas, the grafted αCell-*g*-PHBV composites showed comparable E to neat PHB, suggesting that the reinforcement of αCell fibers was improved *via* grafting. Moreover, the increased E of the polymer matrix due to crosslinking between polymer chains (see Fig. 1) would partially contribute to the E increase of grafted composites.

The ductility reflected by ε values was significantly higher for PHBV based composites, which contributed to higher flexibility of PHBV (22% HV) than PHB homopolymers.[32] Work on PHB/PHBV-flax fiber composites showed higher values of ε for PHBV based composites than PHB based composites.[34] For composites made from PHB or PHBV, σ at the ultimate yield point was increased with the addition of αCell fibers accompanied with a decrease in ε. In comparison with PHB and its composites the copolymer PHBV based composites showed a somewhat lower σ, around 12 MPa. For the grafted composites (αCell-*g*-PHB and αCell-*g*-PHBV), higher E and ε were obtained when compared to their simple blends. This finding suggests that grafting didn't just enhance the fiber–polymer matrix interaction but also increased the ductility of the resulting composite due to crosslinking between polymer chains (PHB–PHB and PHBV–PHBV). This was possibly caused by a lower degree of crystallinity of cellulose and the bioplastic as discussed in the previous section (Table 3). The toughness of all samples was assessed by their EAB values (Table 4). Neat PHB and PHBV showed respective toughness of 0.33 and 0.45 J, indicating that the PHBV copolymers had an improved toughness than PHB. EAB was also shown to increase with addition of 20% αCell fibers. For example, the EAB of the simple blends, αCell-PHB and αCell-PHBV, were 0.41 and 0.45 J, respectively. A similar result was obtained in a study on the fracture toughness changes due to the addition of 10 to 30% wheat straw fibers into the PHB matrix.[35] Grafting of PHB/PHBV onto αCell improved the toughness significantly ($p < 0.05$) by 46% and 44%, respectively, as compared to their simple blends, αCell-PHB and αCell-PHBV.

According to the Kelly–Tyson theory, the critical fiber length ($L_{c/\alpha Cell}$) is used to evaluate the fibers performing as reinforcement or just filler to the polymer matrix. It is assumed that fiber morphology (length and aspect ratio) would not be influenced significantly during single screw mixing/extrusion processing, for example by shearing, and thus the $L_{c/\alpha Cell}$ can be estimated as follows:

$$L_{c/\alpha Cell} = \frac{\sigma_{\alpha Cell} \times d_{\alpha Cell}}{2\tau} \quad (2)$$

where $\sigma_{\alpha Cell}$ is the αCell fiber strength, $d_{\alpha Cell}$ is the fiber diameter that was averaged based on the weight fraction % ($d_{\alpha Cell}$ = 0.015 mm), and τ is the interfacial bonding strength of fiber and the polymer matrix. $\sigma_{\alpha Cell}$ and τ values were obtained from the literature, respectively at 1.5 GPa and 8.8 MPa.[34] Hence, the $L_{c/\alpha Cell}$ value was calculated to be 1.2 mm. Based on the fiber distribution analysis as shown in Table 2, the size of αCell fibers was lower than the estimated critical length required to give an adequate stress transfer between fiber and the PHB (or PHBV) polymer matrix. This again explained the low σ of simple blended composites without grafting. However, the grafted composites (αCell-*g*-PHB and αCell-*g*-PHBV) showed improved tensile properties due to better stress transfer caused by the newly formed bonds (Fig. 1) between the fiber and the polymer.

2.6. Thermal properties of the bioplastics and biocomposites

2.6.1. Thermal degradation behavior. Thermal degradation for neat PHB and PHBV and biocomposites was investigated by thermogravimetric analysis (TGA) and the degradation temperatures are given in Table 5. Neat PHB and PHBV started (T_{onset}) to degrade at 263 and 250 °C, and completed degradation (T_{comp}) at 303 and 292 °C, respectively. The HV units in PHBV did not improve the thermal stability of the polymer, which agrees with previous research.[36] Degradation (98% mass loss) occurred in one step for the neat polymers. This was ascribed to chain scission and hydrolysis mechanisms of PHB and PHBV, resulting in a lower molar mass fragments and the formation of crotonic acid.[36] All the biocomposite samples showed two degradation stages, of which the first stage was ascribed to the PHB/PHBV degradation while the second stage was from αCell degradation. The T_{onset} for the αCell-PHB and αCell-PHBV blends was close to neat PHB/PHBV, and 80% of the biocomposite samples degraded in the first stage, aligning to the formulation (αCell : PHB = 1 : 4; αCell : PHBV = 1 : 4). These data indicated that simple blending of αCell fibers with PHB/PHBV did not improve the thermal stability of the polymer matrix. These results are consistent with the findings for PHB and cotton fiber blends.[26] However, the grafted biocomposites (αCell-*g*-PHB and αCell-*g*-PHBV) had a higher T_{onset} by >10 °C than neat PHB and PHBV. The temperature of maximum decomposition rate (T_{max}) in the first stage for sample αCell-*g*-PHB was >10 °C higher than T_{max} of neat PHB (285 °C). Furthermore, the T_{max} in the second stage due to αCell ($T_{\alpha Cell}$) component degradation was also increased compared to αCell-PHB blends. Similar results were obtained for PHBV based biocomposites. Grafting modification improved the thermal stability for both the reinforcement (αCell) and the polymer matrix (PHB and PHBV). Grafting between αCell and the polymer matrix and a small amount of cross-linked PHB or PHBV resulted in forming more C–C bonds (Fig. 1b and c), which would require more energy/thermal input to decompose the resultant grafted biocomposites.

2.6.2. Different scanning calorimetry (DSC) analysis. The thermal events of glass, crystallization, melting transitions of neat PHB/PHBV, simple blends, and grafted biocomposites were studied using DSC. Fig. 6 shows the DSC thermograms for neat PHB and PHBV, and their biocomposites in the temperature range of −30 to 180 °C. Thermal transitions as well as the degree of crystallinity (X_c %, eqn (10)) of the materials are given in Table 6. Neat PHB showed a glass transition (T_g = 4.9 °C) and double endothermic peaks (T_{m1} = 159 °C and T_{m2} = 169 °C, labeled from low to high temperatures) corresponding to melting points in the second heating scan (Fig. 6). The addition of 20 wt% αCell to neat PHB (αCell-PHB blend) resulted in a slight increase in T_g (5.3 °C), while the grafted αCell-*g*-PHB biocomposites increased T_g by 2 °C. The X_c % of αCell-PHB and αCell-*g*-PHB biocomposites was reduced by 2.4% and 10.4%, respectively, as compared to neat PHB (53.4%). The reduction in crystallinity (or amorphous phase increase) observed by DSC agreed with results of FTIR and WAXD analyses (Table 4).

The T_g is directly associated with the macromolecular mobility of polymer chains, hence, a lower X_c % will require less energy to move the polymer chains in the amorphous phase. Therefore, a lower T_g is expected to transit the polymer from a glassy to a rubbery state if only polymer matrix itself was modified by DCP as reported in our previous studies.[37] However, higher T_g was observed for αCell-PHB and αCell-*g*-PHB biocomposites, which was possibly due to the limited polymer molecular chain mobility from the rigid αCell fibers. Bhardwaj *et al.*[38] found a similar trend for T_g of recycled fibers reinforced PHBV composites. In αCell-*g*-PHB, extra C–C bonds due to grafting between the fibers and the polymer matrix would provide further restrictions in the polymer chain mobility as compared to αCell-PHB, and hence T_g was shifted to a higher temperature.

During DSC analysis, the melt peaks, T_{m1} and T_{m2}, of αCell-PHB were increased slightly from 159 to 161 °C and from 169 to 171 °C, respectively, as compared to neat PHB. While the αCell-*g*-PHB composites showed T_{m1} and T_{m2} values respecti-

Table 5 Thermal degradation temperatures of PHB and PHBV based biocomposites obtained from TGA data[a]

		T_{max} (°C)		
Samples	T_{onset} (°C)	T_{PHB}/T_{PHBV} (°C)	$T_{\alpha Cell}$ (°C)	T_{comp} (°C)
α-Cellulose	303		342	400
PHB	263	285		303
αCell-PHB	264	287	328	358
αCell-*g*-PHB	277	298	335	364
PHBV	250	270		292
αCell-PHBV	253	273	334	362
αCell-*g*-PHBV	260	284	340	363

[a] T_{onset} = beginning weight loss; T_{max} = the temperature of maximum decomposition rate; T_{PHB}, T_{PHBV} = maximum decomposition rate of PHB and PHBV degradation stage (the 1st stage of biocomposites), respectively; $T_{\alpha Cell}$ = maximum decomposition rate of αCell degradation (the 2nd stage of biocomposites); T_{comp} = 100% mass loss onset point.

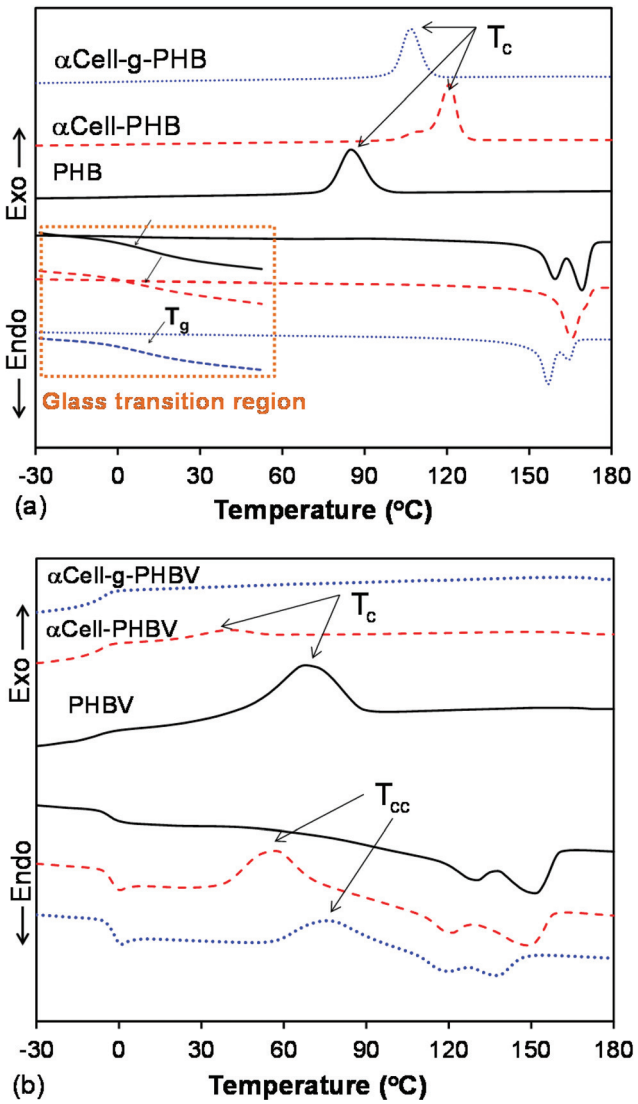

Fig. 6 DSC cooling and the 2nd heating curves of (a) PHB, αCell-PHB and αCell-*g*-PHB and (b) PHBV, αCell-PHBV and αCell-*g*-PHBV samples.

Table 6 Crystallization temperature (T_c), peak temperatures of the low- and high-temperature endotherms (T_{m1} and T_{m2}), and degree of crystallinity (X_c %). Standard deviation values are given in parentheses

Samples	T_g (°C)	T_{m1} (°C)	T_{m2} (°C)	X_c (%)	T_c (°C)	T_c (°C)	ΔH_c (J g^{-1})
Neat PHB	4.9	159	169	53.4 (1.2)	85	ND	67
αCell-PHB	5.3	161	171	50.0 (0.5)	121	ND	63
αCell-*g*-PHB	6.9	155	164	43.0 (2.3)	103	ND	55
Neat PHBV	−4.0	129	153	17.8 (0.5)	67	ND	27
αCell-PHBV	−2.0	126	151	16.8 (1.1)	39	56.4	22
αCell-*g*-PHBV	−0.5	118	135	4.60 (0.2)	ND	76.5	ND

ND: not detected.

vely at 155 and 164 °C. This reduction is likely caused by the broadening molar mass distribution of the polymer matrix due to grafting/cross-linking between polymer chains. A similar trend was observed for T_g, T_m's and X_c % for PHBV and its biocomposite samples (Table 6). However, a more apparent change was seen in the grafted αCell-*g*-PHBV material. This could be contributed to the chemical structure of PHBV/PHB polymers[26] and the higher GE% of PHBV.

DSC can easily detect the significant heat release accompanying the exothermic crystallization process of PHB and PHBV. The T_c is an important thermal parameter to describe the crystallization behavior of fiber and plastic composites (Fig. 6 and Table 6). A sharp crystallization peak was observed for all PHB-based samples and neat PHBV in the cooling scan. An increase in T_c was observed when αCell fibers were incorporated into the PHB matrix (T_c = 85 °C). This suggested that the αCell fibers induced nucleation of PHB and initiated the crystallization at higher temperature (*i.e.* >121 °C) from melt. Grafting resulted in a decrease in T_c (103 °C) of αCell-*g*-PHB as compared to the blended αCell-PHB material. The corresponding enthalpy (ΔH_c) of αCell-*g*-PHB during crystallization was reduced by 12% due to grafting. This reduction was most likely due to the lower X_c % of PHBV (or PHB) in the grafted biocomposites (Table 6). The exothermic peak of neat PHBV was broader than PHB, which indicated nucleation and crystal growth were much slower in PHBV. This finding agrees with the literature.[39] The T_c of PHBV in αCell-PHBV was reduced significantly by 28 °C as compared to that of neat PHBV. This indicated that the addition of fibers resulted in a slower diffusion and migration of PHBV copolymer chains to the surface of the nucleation point, thus decreasing T_c during cooling of the αCell-PHBV melt. For the grafted biocomposites, αCell-*g*-PHBV, no exothermic crystallization peak (T_c) was observed by DSC in the cooling scan. The reduction in the X_c %, T_m's, and T_c was in agreement with the results reported in the case of poly(ε-caprolactone) (PCL) reinforced with PCL diol grafted cellulose nanocrystals using toluene 2,4-diisocyanate as the coupling agent.[40] In addition, an exothermal (cold crystallization) peak (T_{cc}) was observed in the heating scan of PHBV based composites (Fig. 6b). This peak was shifted from 56 °C to higher temperature (77 °C) due to grafting, indicating the delay of crystallization kinetics (increased crystallization rate) with incorporation of cellulose fibers and grafting crosslinks.

2.6.3. Dynamic flexural properties. Dynamic mechanical analysis (DMA) was performed on PHB, PHBV and their composites in a three-point bending mode to determine the storage modulus (E') which determines the dynamic rigidity of a material. The E' values of the samples at 30, 50 and 70 °C are given in Table 7. The E' values (30 °C) of PHB increased by 33% and 60%, respectively by simple addition of αCell and grafting of αCell, respectively. The αCell-PHBV and αCell-*g*-PHBV biocomposites had also shown significantly increased E' values by 88 and 127%, respectively, as compared to neat PHBV. PHB had a higher E' due to its high brittleness than PHBV. The higher E' values for the grafted composites could be contributed to an improved compatibility and dispersion of αCell fibers in the PHB/PHBV matrix as compared to their blends (αCell-PHB and αCell-PHBV). Better stress transfer

Table 7 Comparative storage moduli (E') at selected temperatures, tan δ and adhesion factor (A) near to room temperature (30 °C) of neat PHB and PHBV based samples. Standard deviation values are given in parentheses

	Storage modulus E' (MPa)			tan δ				
Samples	30 °C	50 °C	70 °C	tan $\delta_{30\ °C}$	tan $\delta_{50\ °C}$	tan $\delta_{70\ °C}$	V_f (%)	$A_{30\ °C}$
Neat PHB	1797	1466	1276	0.076	0.037	0.040	0	—
αCell-PHB	2395	2073	1820	0.070	0.043	0.050	16 (0.5)	1.25 (0.20)
αCell-*g*-PHB	2869	2255	1934	0.040	0.035	0.054	15 (1.2)	0.28 (0.00)
Neat PHBV	630	548	439	0.090	0.065	0.074	0	—
αCell-PHBV	1182	742	486	0.065	0.068	0.090	16 (0.5)	0.72 (0.14)
αCell-*g*-PHBV	1432	985	706	0.050	0.080	0.104	15 (1.2)	0.32 (0.02)

The differences of moduli and tan δ between duplicates were less than 20 MPa and 0.005, respectively; hence standard deviation was not reported.

between the αCell and PHB/PHBV interfaces of the grafted composites would also improve the rigidity of either PHB or PHBV composites.

The loss tangents (tan δ) of the various samples at 30, 50 and 70 °C are given in Table 7 as well. Tan δ values were shown to have a minimum at 50 °C. For both PHB and PHBV based composites their tan δ values were less than their matrix, especially <30 °C. According to our previous findings of the fiber–matrix interfacial bonding,[9,25] the reduction of tan δ could indicate better interfacial adhesion of these two phases in grafted biocomposites as compared to their simple blends without being grafting modified.

The interfacial bonding between wood fiber and the polyethylene matrix was successfully evaluated by the adhesion factor (A) (eqn (11)).[9] A values derived from DMA data at 30 °C are given in Table 7. Lower A values of the grafted composites was an indicator of improved interfacial interaction between the two phases, αCell and PHB or PHBV, as compared to their blend. These data provided supportive evidence that an improved interaction was achieved by grafting.

2.7. Dynamic rheological properties

The polymer melt properties of the biocomposites were determined by dynamic parallel plate rheometry. Fig. 7 shows the dynamic elastics and viscous moduli (G' and G'') of PHB (175 °C) and PHBV (170 °C) based materials under isothermal conditions. For the PHB based composites both G' and G'' were shown to increase with frequency (ω, rad s^{-1}). At lower ω, G'' was higher than G' for PHB and the simple blended composite (αCell-PHB). This indicated that these samples were more liquid-like, although the incorporation of αCell made the resulting composites slightly more elastic which was reflected by the less difference between G'' and G' values. However, grafting improved the G' slightly compared to the simple blends (see Fig. 7a, $G' > G''$), suggesting that the grafted PHB onto αCell showed good elastic properties. For instance, G' was increased from 12 Pa (PHB) to 1000 Pa by addition of αCell and further improvement to 1400 Pa was obtained by grafting (αCell-*g*-PHB). PHBV, αCell-PHBV and αCell-*g*-PHBV showed higher G' and G'' values than PHB series which clearly showed

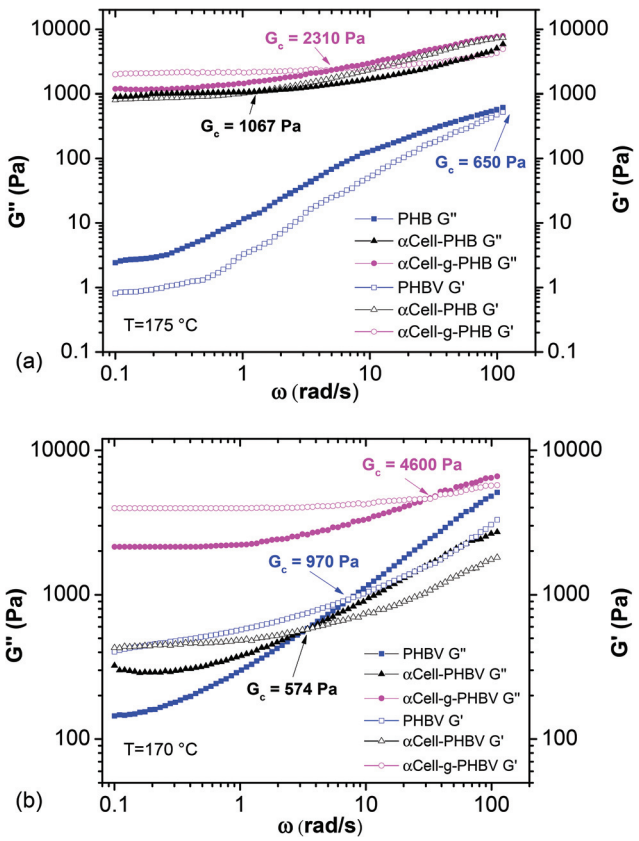

Fig. 7 Effect of grafting on dynamic rheology storage (G') and loss (G'') moduli of (a) PHB, αCell-PHB, and αCell-g-PHB samples at 175 °C and (b) PHBV, αCell-PHBV and αCell-g-PHBV samples at 170 °C. G_c is the crossover modulus when $G' = G''$.

that the PHBV copolymer had relatively better melt strength. At lower frequency, *i.e.* $\omega < 10$ rad s^{-1}, $G' > G''$ was observed for PHBV and its composites, suggesting that the PHBV (22 mol% HV) has better melt strength (higher melt viscosity) than PHB. Conflicting results were observed in other studies on the PHBV with lower HV content (12 mol%).[41] In addition, due to a relatively longer chain of HV as compared to HB more degrees of

chain entanglements in PHBV would be presented as compared to PHB. As found in previous research studies,[37,42] the melt elasticity is positively proportional to the molecular chain entanglement and the degree of long chain branching. Although pure PHBV is a linear polymer, the presence of HV monomeric units could provide long chain branching structures. Compared to pure PHB homopolymers, PHBV can be considered as a branched form of PHB, and thus PHBV and its composites showed $G' > G''$. A similar trend ($G' > G''$) was observed between the long chain branched and linear polyethylene samples.[42]

The polymer melt of the copolymer PHBV had better elasticity than that of PHB (Fig. 7b). The addition of αCell to PHBV increased its G'' by 30%. The effect of grafting of αCell onto PHBV further increased G' (5-fold) and G'' (7-fold) significantly as compared to the blend. The improvements of PHBV properties, relative to PHB, are most likely due to the higher grafting efficiency of PHBV when using the same reactive parameters.

The cross-over modulus ($G_c = G' = G''$) of grafted PHB and PHBV biocomposites shifted towards higher ω. The G_c was increased from 670 Pa for PHB to 1070 Pa by the addition of αCell and was further increased to 2300 Pa by grafting. A similar trend was also observed for the PHBV composite series. The mean relaxation time (at G_c), which is the ratio of the elastic to the viscous response,[43] was increased for PHB based composites whereas it was decreased for PHBV based composites due to grafting. This difference might be mainly due to the higher molecular weight of PHBV as well as the fraction of a crosslinked polymer (PHB–PHB, PHBV/PHBV) in the grafted composites. This can result in higher molar mass distribution of grafted PHBV based composites than that of PHB based composites.

αCell-*g*-PHBV behaved like a solid with a G' of about 5 kPa. This could be partially due to long chain branching between crosslinked PHBV (or PHB) chains. There was less of a magnitude increase in moduli for αCell-PHB composites as compared to αCell-PHBV due to grafting. This further indicated the higher grafted efficiency of PHBV based composites with the incorporation of the same peroxide concentration. The relatively lower degree of elasticity for PHB and PHBV compared with their composites was likely caused by their higher chain stiffness, and this phenomenon agrees with their higher T_m values. Therefore, peroxide induced free radical initiation to create crosslinks and grafting is a practical approach to improve the industrial melt processability of PHB and PHBV as well as their biocomposites.

3. Experimental

3.1. Materials

Lodgepole pine (*Pinus contorta*) lumber was sourced locally (Southern Idaho, USA). The lumber was chipped and then Wiley-milled to pass through a 40 mesh screen. Wood fiber (500 g) was extracted with acetone (3 L, 99.5%, Macron Fine Chemicals) to yield 8.0 g of extractives. Air dried extractives of free wood fiber (100 g batches) were treated with 3.2 L deionized water containing 30 g $NaClO_2$ (99%, Tech. Grade, Ricca Chemicals, USA) and acetic acid (20 mL, 99.7%, Fisher ACS, USA) at 70 °C for 1 h, and this was repeated four more times to a total of 6 h.[44] The holocellulose fibers (150 g batch) were then extracted with 17.5% NaOH (4 L) solution at 20 °C with constant stirring for 5 h to afford αCell fibers by removing the hemicelluloses. The αCell was recovered by filtering through a polypropylene screen (100 mesh) and washed exhaustively with water under vacuum. Then, 10% aqueous acetic acid (2 L) was added to the αCell and left to soak for 5 min. The αCell fiber was then washed extensively with water (1 L, 10–15 times) until neutral pH. Finally, αCell was rinsed with acetone to accelerate drying, and then dried in a vacuum oven (>24 h) to <0.5% moisture content. This method yielded 55% αCell based on the initial dry weight of wood.

Poly-3-hydroxybutyrate (PHB: M_w = 290 000 g mol^{-1}) and poly(3-hydroxybutyrate-*co*-3-hydroxyvalerate) (PHBV: 22 mol% HV content; M_w = 400 000 g mol^{-1}) powder were obtained from Tianan Biopolymer Inc. (Ningbo, China). These PHAs are non-nucleated grades without any additives. Dicumyl peroxide (DCP: 98%) was a product of Sigma-Aldrich (USA). CH_2Cl_2 (J.T. Baker, USA) was used as received.

3.2. Biocomposites processing

The PHB and PHBV based composites were prepared according to our previous work.[26] Briefly, αCell, PHB and PHBV were separately coated with DCP in acetone solution (4–8 mg mL^{-1}) for 30 min, and then air dried followed by drying in a vacuum oven (>24 h) prior to composites processing. DCP coated PHB or PHBV (80%) and αCell (20%; moisture content was <0.5%) were dried and premixed in a beaker. The αCell-*g*-PHB and αCell-*g*-PHBV grafted biocomposites were prepared in a Dynisco Lab Mixer Molder/Extruder (LMM) using the reactive extrusion process and mixed (500 rpm) for time t_R and then extruded into strands (1 mm Ø) or injection molded into rectangular bars (60 × 9 × 2 mm^3), dog-bones or discs. The processing temperature was 175 °C for PHB and 170 °C for PHBV based materials. The grafting efficiency (GE%) was evaluated by extracting the non-soluble copolymerized gel fraction using Soxhlet extraction for 24 h in chloroform to remove any non-reacted PHB. The extract was then filtered through a nylon screen with a pore size of about 450 μm which was large enough to allow nonreacted cellulose fibers to pass through. The conditions (DCP concentration and reaction time t_R) at which maximum grafted copolymer gel yield were considered to be optimized parameters used to prepare grafting modified biocomposites.[19] Simple blends of αCell and PHB (αCell-PHB) or PHBV (αCell-PHBV) without the addition of DCP were prepared as control strand and rectangular bar samples.

3.3. Characterization

3.3.1. α-Cellulose fiber analysis. Sieve analysis was performed on the isolated αCell fibers (10 g) using standard test sieves (40, 60, 80, 100, and 200 mesh and pan) on a Soil Test

Inc., Model CL-300B shaker for 10 min, and the weight distribution was determined. The average length and diameters of the isolated αCell fibers in each fraction were averaged from two hundred fibers dyed with safranin and observed by optical microscopy (Olympus BX51 in bright field mode and images captured using an Olympus DP70 digital camera).

The chemical composition of the original wood and αCell fibers for CH_2Cl_2 extractive, lignin (acid soluble and Klason lignin), carbohydrate (hemicellulose and cellulose), and ash compositions was determined according to the methods described in detail by Liang and McDonald.[45] More specifically, the wood and αCell fiber samples (4–5 g) were Soxhlet extracted with CH_2Cl_2 (150 mL) for 16 h in accordance with ASTM D 1108-9623 and the extractives were determined gravimetrically. The lignin content was determined as acid insoluble and acid soluble lignin on extractive free samples. Carbohydrate analysis was performed on the 2-stage acid-hydrolyzates according to ASTM E 1758-01.26 with slight modification. The dried sample (200 mg) was incubated in 72% H_2SO_4 (2 mL) for 1 h at 30 °C, then diluted into 4% H_2SO_4, and subjected to secondary hydrolysis in an autoclave (117 kPa and 121 °C) for 30 min. The hydrolyzate was filtered through a sintered crucible to obtain the acid insoluble (Klason lignin) residue content gravimetrically after it was oven dried at 104 °C. An aliquot of the hydrolysate (made up to 250 mL) was taken to determine the acid soluble lignin content at 205 nm using an absorption coefficient of 110 L g^{-1} cm^{-1} on a Beckman DU640 spectrometer. To the hydrolysate (5 mL) inositol (1 mL, 0.5 mg mL^{-1}) was added as an internal standard, and then $PbCO_3$ (0.16 g) was added to remove the sulfate, and centrifuged. The supernatant was deionized by passing through an ion exchange resin cartridge (containing Amberlite IR-120 H^+ (0.5 mL) and Amberlite IRA35 OH^- (0.5 mL)) and filtered through a 0.45 μm syringe filter (nylon, Fisher Scientific) into an HPLC vial. Monosaccharides were quantified by HPLC using two Rezex RPM columns in series (7.8 mm × 30 cm, Phenomenex) at 85 °C equipped with a differential refractive index detector (Waters Associates model 2414) on elution with water (0.5 mL min^{-1}). The chromatographic data were analyzed using N2000 software (Science Technology Inc., China). The ash content of lodgepole pine wood and isolated αCell fibers were determined by furnacing samples at 600 °C according to ASTM D 1102-84.

3.3.2. Surface morphology of composites. Biocomposite bar samples were microtomed into 100 μm thick specimens and coated with carbon and gold. The prepared samples were investigated at 500× and 200× magnifications using a LEO Gemini field emission SEM operating at 4 kV under high vacuum.

3.3.3. Surface chemistry by FTIR spectroscopy. αCell fibers, PHB, PHBV, and biocomposite samples were characterized by FTIR spectroscopy using a Thermo Nicolet iS5 FTIR spectrometer (ZnSe attenuated total reflection (ATR) probe (iD5)). Samples (in triplicate) were analyzed after vacuum drying. The absorbance spectra were baseline corrected and averaged using software Omnic v9.0 (Thermo Scientific).

The total crystallinity index (TCI) of αCell fibers, and the quantitative crystallinity indices of the carbonyl (C=O stretching) group ($I_{C=O,\ PHB/PHBV}$) and C–O stretching ($I_{C-O,\ PHB/PHBV}$) of PHB/PHBV polymers before and after grafting were determined as follows:

$$\mathrm{TCI} = A_{1370}/A_{2900} \tag{3}$$

$$I_{C=O,PHB/PHBV} = A_{1720}/A_{1740} \tag{4}$$

$$I_{C-O,PHB/PHBV} = A_{1230}/A_{1450} \tag{5}$$

where A_{1370} and A_{2900} are the areas of αCell peaks at 1370 and 2900 cm^{-1}, respectively, and A_{1230}, A_{1450}, A_{1720} and A_{1740} are the areas of the peaks near to 1230, 1450, 1720 and 1740 cm^{-1} from PHB (or PHBV) molecular chains, respectively. All band areas were obtained by peak fitting processing using IGOR Pro v6 (WaveMetrics) software.[9] Gaussian functionality was employed for peak fitting using selected peak width at half height (FWHM) values.

3.3.4. Crystallinity characterized by WAXD. The crystalline structures of αCell fibers and injection molded neat PHB/PHBV and biocomposite samples were characterized by WAXD (Siemens D5000 diffractometer) at room temperature. The instrument was set up with a rotating Cu Kα2 X-ray tubes operating at 40 kV with a current density of 30 mA. Scanning was performed over 2θ ranging from 5 to 50° with steps of 0.2°. The collected diffractograms were processed and the peak of interest was fitted/deconvoluted (Gaussian function) using IGOR Pro v6 software. The intensity of each peak identified by peak fitting was mathematically computed. The methods to determine the crystallinity index of αCell ($\mathrm{CrI}_{\alpha\mathrm{Cell}}$), PHB ($\mathrm{CrI}_{\mathrm{PHB}}$),[26] and PHBV ($\mathrm{CrI}_{\mathrm{PHBV}}$) are according to:

$$\mathrm{CrI}_{\alpha\mathrm{Cell}} = (1 - (I_{\mathrm{am}}/I_{002})) \times 100 \tag{6}$$

where I_{am} is the intensity of the peak at $2\theta = 18°$ and I_{002} is the maximum intensity of the (002) plane diffraction.

The PHB and PHBV crystallinity index was calculated according to:

$$\mathrm{CrI}_{\mathrm{PHB}} = I_{17}/I_{\text{total-PHB}} \times 100 \tag{7}$$

$$\mathrm{CrI}_{\mathrm{PHBV}} = I_{17}/I_{\text{total-PHBV}} \times 100 \tag{8}$$

where I_{17} is the intensity of the peak close to $2\theta = 17°$ and I_{total} is the total intensity of all crystalline peaks of PHB ($I_{\text{total-PHB}}$) or PHBV ($I_{\text{total-PHBV}}$).

The crystal size dimension D_{hkl} was estimated as well by Scherrer's formula:[46]

$$D_{hkl} = K \times \lambda/(\beta_{1/2} \times \cos\theta) \tag{9}$$

where K is the crystal shape constant, λ is the X-ray wavelength (λ = 0.1542 nm, $\beta_{1/2}$ is the FWHM, ≈2 Deg.) obtained by IGOR Pro, when peak fitting was conducted with the Gaussian function, and θ is the diffraction angle.

3.3.5. Tensile testing. All injection molded microtensile (dog-bone) samples (10 replicates) were conditioned at 65% relative humidity at 23 °C for at least 7 d. Tensile tests were

performed according to ASTM Standard D1708 using an Instron 5500R-1132 universal test machine with a constant strain rate of 1 mm min^{-1}, 5 kN load cell, and the strain was measured using an extensometer (model 3542, Epsilon Technology Corp.). The density of injection molded samples was calculated based on the initially conditioned dry weight and dimensions.

3.3.6. Thermal analysis. TGA was performed on a TGA-7 (Perkin-Elmer) instrument. Samples (3–5 mg, in duplicates) were heated from 50 to 900 °C at a rate of 20 °C min^{-1} under nitrogen (30 mL min^{-1}). Data were analyzed with replicated curves and were averaged using Pyris v8 software (Perkin Elmer).

DSC measurement was performed on neat PHB/PHBV and biocomposites (4–6 mg, in duplicate) using a TA Instruments model Q200 DSC with refrigerated cooling. The samples were (i) equilibrated at 40 °C (3 min) then ramped to 190 °C at 10 °C min^{-1}, held isothermally for 5 min to remove any thermal history, (ii) cooled to −50 °C at a rate of −10 °C min^{-1} and held isothermally for 3 min, and (iii) reheated to 190 °C at 10 °C min^{-1} to record the heating scan. Data were analyzed using TA Universal Analysis v4.4A software. Glass transition (T_g) and melting temperatures (T_m) were determined from the peaks of the second heating scan, while crystallization transition temperature (T_c) was obtained from the peak of the cooling scan. The degree of crystallinity (X_c %) of PHB and PHBV was calculated as follows:

$$X_c\% = \Delta H_m/(\Delta H_0 \times W_f) \times 100 \quad (10)$$

where ΔH_m is the melting enthalpy of sample (PHB and PHBV polymers), and ΔH_0 is melting enthalpy in J g^{-1} of 100% crystalline PHB (146 J g^{-1}),[37,47] and W_f is the weight fraction of PHB or PHBV (80%) in biocomposite samples. Note: if the differences of transition temperatures between duplicates were less than 0.2 °C, standard deviation will not be reported.

DMA measurements were conducted on biocomposite samples using a TA Q800 Instruments. At least duplicate rectangular injection molded rectangular bars (60 × 9 × 2 mm^3) were tested using a 3-point bending fixture (50 mm span). Samples were heated from 30 to 150 °C at 2 °C min^{-1}, 0.05% strain, and at a single frequency of 1 Hz. Data were analyzed by TA Universal Analysis v4.4A software.

The αCell/PHB and αCell/PHBV interfacial adhesion was evaluated by an adhesion factor (A) which was calculated from DMA results at 30 °C as follows:[9,48]

$$A = (1/(1 - V_f))\ (\tan \delta_c/\tan \delta_m) - 1 \quad (11)$$

where c and m subscripts represent biocomposites and the polymer matrix (PHB and PHBV), and V_f is the fiber volume fraction which was determined in accordance to ASTM standard D2584:

$$V_f = (W_f\rho_m)/(W_f\rho_m + W_m\rho_f) \quad (12)$$

where W_f is the weight of αCell fibers which is 20%, W_m is the weight of the polymer matrix which is 80%, ρ_f is the density of fibers (ρ_f = 1.5 g cm^{-3}),[49] and ρ_m is the density of matrix (ρ_m values of PHB and PHBV are 1.18 and 1.10 g cm^{-3}, respectively). V_f values of PHB and PHBV based composites were 16% and 15%, respectively.

3.3.7. Rheological analysis. The dynamic rheological measurements (G', G'' and η^*) were determined using a Bohlin CVO 100 rheometer, a parallel plate (25 mm Ø), in an oscillating shear mode with an ETC module on molded disc (2 mm × 25 mm Ø) samples. Experiments were performed in the linear viscoelastic region. For PHB and PHBV based materials, measurements were carried out at 175 and 170 °C, respectively, in the frequency range of 0.1 to 100 rad s^{-1} at an applied isostrain of 0.5%. Data were analyzed using the Bohlin rheology v6.51 software.

4. Conclusion

The use of DCP in grafting modification of αCell/PHB and αCell/PHBV biocomposites *via* an *in situ* reactive extrusion process was successful to achieve beneficial properties. Surface morphology by SEM revealed better compatibility of cellulose in the polymer (PHB and PHBV) matrix of the resultant biocomposites due to grafting modification as compared to blends. The tensile tests showed that the grafting increased the toughness and flexibility of biocomposites due to the enhanced fiber–polymer matrix interaction and lower degree of crystallinity as compared to neat polymers and simple blends. The degree of crystallinity of the composites was reduced through grafting, which was reflected by the crystallinity indices estimated from quantitative FTIR and WAXD analyses. Grafting was found to have a significant influence on the thermal properties (*e.g.* stability) of αCell-*g*-PHB/PHBV biocomposites. Lower processing temperatures and shorter cycle times during melt processing could be achieved and further minimize degradation. Grafting improved the interfacial bonding between αCell fibers and the polymer matrix as determined by the adhesion factor. It can be concluded that this approach afforded cellulose reinforced bioplastic composite materials with significantly improved mechanical and thermal properties by chemically grafting the fibers with the matrix to improve stress transfer. This grafting modification was achieved *via* a one-step reactive extrusion process and can provide a sustainable strategy to utilize cellulose fibers derived from various renewable resources including any at-risk intermountain wood species to create value added products. This developed technique can be applied to PHB/PHBV biosynthesized from waste substrates by mixed microbial consortia to lower the cost of these materials which will help their applications as bulk materials.

Acknowledgements

The authors would like to acknowledge (i) the financial support from a USDA-Forest Products Laboratory Grant 08-

JV-111111, (ii) USDA-CSREES Grant 2007-34158-17640 for supporting the DSC and DMA, and (iii) ThermoScientific for the FTIR spectrometer.

References

1 G.-Q. Chen and M. K. Patel, *Chem. Rev.*, 2012, **112**, 2082–2099.
2 R. U. Halden, *Annu. Rev. Public Health*, 2010, **31**, 179–194.
3 D. Garlotta, *J. Polym. Environ.*, 2001, **9**, 63–84.
4 T. Mekonnen, P. Mussone, H. Khalil and D. Bressler, *J. Mater. Chem.A*, 2013, **1**, 13379.
5 J. Lunt, *Polym. Degrad. Stab.*, 1998, **59**, 145–152.
6 M. Yamaguchi and K. Arakawa, *Eur. Polym. J.*, 2006, **42**, 1479–1486.
7 R. M. Rasal, A. V. Janorkar and D. E. Hirt, *Prog. Polym. Sci.*, 2010, **35**, 338–356.
8 A. Youngblood, J. Zhu and C. T. Scott, Presented in part at the National Silviculture Workshop, Boise, Idaho, 15–18 June, 2009.
9 L. Wei, A. G. McDonald, C. Freitag and J. J. Morrell, *Polym. Degrad. Stab.*, 2013, **98**, 1348–1361.
10 K. Suzuki, A. Sato, H. Okumura, T. Hashimoto, A. N. Nakagaito and H. Yano, *Cellulose*, 2013, **21**, 507–518.
11 C. Fonseca-Valero, A. Ochoa-Mendoza, J. Arranz-Andrés and C. González-Sánchez, *Composites, Part A*, 2015, **69**, 94–104.
12 M. Pöllänen, M. Suvanto and T. T. Pakkanen, *Compos. Sci. Technol.*, 2013, **76**, 21–28.
13 A. K. Bledzki and J. Gassan, *Prog. Polym. Sci.*, 1999, **24**, 221–274.
14 M. Bengtsson, P. Gatenholm and K. Oksman, *Compos. Sci. Technol.*, 2005, **65**, 1468–1479.
15 L. C. Tomé, R. J. B. Pinto, E. Trovatti, C. S. R. Freire, A. J. D. Silvestre, C. P. Neto and A. Gandini, *Green Chem.*, 2011, **13**, 419.
16 A. Gandini, *Green Chem.*, 2011, **13**, 1061.
17 O. Faruk, A. K. Bledzki, H.-P. Fink and M. Sain, *Prog. Polym. Sci.*, 2012, **37**, 1552–1596.
18 M. John and S. Thomas, *Carbohydr. Polym.*, 2008, **71**, 343–364.
19 D. Roy, M. Semsarilar, J. T. Guthrie and S. Perrier, *Chem. Soc. Rev.*, 2009, **38**, 2046–2064.
20 L. Yu, K. Dean and L. Li, *Prog. Polym. Sci.*, 2006, **31**, 576–602.
21 S. A. Madbouly, J. A. Schrader, G. Srinivasan, K. Liu, K. G. McCabe, D. Grewell, W. R. Graves and M. R. Kessler, *Green Chem.*, 2014, **16**, 1911.
22 L. Wei, S. Liang and A. G. McDonald, *Ind. Crops Prod.*, 2015, **69**, 91–103.
23 D. Roy, M. Semsarilar, J. T. Guthrie and S. Perrier, *Chem. Soc. Rev.*, 2009, **38**, 2046–2064.
24 A. Carlmark, E. Larsson and E. Malmström, *Eur. Polym. J.*, 2012, **48**, 1646–1659.
25 N. Le Moigne, M. Longerey, J.-M. Taulemesse, J.-C. Bénézet and A. Bergeret, *Ind. Crops Prod.*, 2014, **52**, 481–494.
26 L. Wei, A. G. McDonald and N. M. Stark, *Biomacromolecules*, 2015, **16**, 1040–1049.
27 T. A. Clark, K. L. Mackie, P. H. Dare and A. G. McDonald, *J. Wood Chem. Technol.*, 1989, **9**, 135–166.
28 J. Yang, J.-J. Zhao, F. Xu and R.-C. Sun, *ACS Appl. Mater. Interfaces*, 2013, **5**, 12960–12967.
29 K. Joseph and S. Thomas, *Polymer*, 1996, **37**, 5139–5149.
30 W. J. Orts, R. H. Marchessault, T. L. Bluhm and G. K. Hamer, *Macromolecules*, 1990, **23**, 5368–5370.
31 K. Sudesh, H. Abe and Y. Doi, *Prog. Polym. Sci.*, 2000, **25**, 1503–1555.
32 L. Wei, N. M. Guho, E. R. Coats and A. G. McDonald, *J. Appl. Polym. Sci.*, 2014, **131**, 40333, DOI: 10.1002/app.40333.
33 D. Maldas and B. V. Kokta, *J. Adhes. Sci. Technol.*, 1994, **8**, 1439–1451.
34 N. M. Barkoula, S. K. Garkhail and T. Peijs, *Ind. Crops Prod.*, 2010, **31**, 34–42.
35 M. Avella, G. La Rota, E. Martuscelli and M. Raimo, *J. Mater. Sci.*, 2000, **35**, 829–836.
36 S. Modi, K. Koelling and Y. Vodovotz, *Eur. Polym. J.*, 2011, **47**, 179–186.
37 L. Wei and A. G. McDonald, *J. Appl. Polym. Sci.*, 2015, **132**, 41724.
38 R. Bhardwaj, A. K. Mohanty, L. T. Drzal, F. Pourboghrat and M. Misra, *Biomacromolecules*, 2006, **7**, 2044–2051.
39 M. Scandola, M. L. Focarete, G. Adamus, W. Sikorska, I. Baranowska, S. Swierczek, M. Gnatowski, M. Kowalczuk and Z. Jedlinski, *Macromolecules*, 1997, **30**, 2568–2574.
40 J. O. Zoppe, M. S. Peresin, Y. Habibi, R. A. Venditti and O. J. Rojas, *ACS Appl. Mater. Interfaces*, 2009, **1**, 1996–2004.
41 E. Ten, D. F. Bahr, B. Li, L. Jiang and M. P. Wolcott, *Ind. Eng. Chem. Res.*, 2012, **51**, 2941–2951.
42 D. Yan, W.-J. Wang and S. Zhu, *Polymer*, 1999, **40**, 1737–1744.
43 D. H. S. Ramkumar and M. Bhatacharya, *Polym. Eng. Sci.*, 1998, **38**, 1426–1435.
44 J. S. Fabiyi, A. G. McDonald, M. P. Wolcott and P. R. Griffiths, *Polym. Degrad. Stab.*, 2008, **93**, 1405–1414.
45 S. Liang and A. G. McDonald, *J. Agric. Food Chem.*, 2014, 140805102128006.
46 L. E. Alexander, *X-ray diffraction method in polymer science*, Wiley-Interscience, New York, 1969.
47 P. J. Barham, A. Keller and E. L. Otun, *J. Mater. Sci.*, 1984, **19**, 2781–2794.
48 J. Kubát, M. Rigdahl and M. Welander, *J. Appl. Polym. Sci.*, 1990, **39**, 1527–1539.
49 W. A. Sisson, in *Cellulose and cellulose derivatives*, ed. E. Ott, Interscience, New York, 1943, ch. 4, vol. 5, p. 214, ch. 3.

